Recurrent Rossby waves and South-eastern Australian heatwaves

S. Mubashshir Ali*[1], Matthias Röthlisberger[2], Tess Parker[3], Kai Kornhuber[4,5], and Olivia Martius[1,56]

1. Oeschger Centre for Climate Change Research and Institute of Geography, University of Bern, Bern, Switzerland,
2. Institute for Atmospheric and Climate Science, ETH Zürich, Zürich, Switzerland,
3. School of Earth, Atmosphere and Environment, Monash University, Clayton VIC, Australia,
4. Lamont Doherty Earth Institute Observatory, Columbia University, New York City, NY, USA, and
55. German Council on Foreign Relations, Berlin, Germany, and
6. Mobiliar Lab for Natural Risks, University of Bern, Bern, Switzerland.

*Corresponding author: mubashshir.ali@giub.unibe.ch

Abstract

In the Northern Hemisphere, recurrence of transient synoptic-scale Rossby wave packets in the same phase over periods of days to weeks, termed RRWPs, may repeatedly create similar surface weather conditions. This recurrence can lead to persistent surface anomalies. Here, we first demonstrate the significance of RRWPs for persistent hot spells in the Southern Hemisphere (SH) using the ERA-I reanalysis dataset and then examine the role of RRWPs and blocks for heatwaves over south-eastern Australia (SEA).

A Weibull regression analysis shows that RRWPs are statistically associated with a significant increase in the duration of hot spells over several regions in the SH, including SEA. Two case studies of heatwaves in SEA in the summers of 2004 and 2009 illustrate the role of RRWPs in forming recurrent ridges (anticyclonic potential vorticity, PV anomalies), aiding in the persistence of the heatwaves. Then, using an observationa weather station-based dataset to identify SEA heatwaves, we find that SEA heatwaves are more frequent than climatology during days with extreme RRWPs activity. over SEA (high R_{SEA}). On days with both RRWPshigh R_{SEA} and heatwaves, a circumglobal zonal wavenumber 4wavenumbers (WN) 4 and 5 anomaly pattern is present in the composite mean of the upper-level PV field, with an anticyclonic PV anomaly over SEA. The Fourier decomposition of the PV and meridional wind velocity fields further reveals that the WN4 and WN5 components in the suitable phase aids in forming the ridge over SEA for days with high R_{SEA}. In addition, we find positiveanomalous blocking frequency anomalies over the Indian and the south Pacific Oceans during SEA heatwaves, which may help to modulate the phase of RRWPs during SEA heatwaves.

1. **Introduction**

Since 1900, extreme heat has been responsible for more fatalities in Australia than all other natural hazards combined (Coates et al., 2014). Heatwaves also exacerbate the risk of wildfires, cause surges in power demand, and increase insurance costs (Hughes et al., 2020; Insurance Council of Australia, 2020). Increasingly frequent and severe heatwaves in the midlatitudes in the recent years (Coumou et al., 2013; Perkins-Kirkpatrick and Lewis, 2020; IPCC 2021) have spurred fruitful research on the atmospheric drivers of heatwaves. Understanding the dynamical mechanisms is particularly important for improving sub-seasonal prediction (Quandt et al., 2017) and for quantifying future changes in heatwaves (Shepherd, 2014; Wehrli et al., 2019).

Several large-scale atmospheric mechanisms and phenomena have been identified as potential drivers of heatwaves in the Northern Hemisphere extra-tropics.(NH) extratropics. They include blocking anticyclones (e.g., Barriopedro et al., 2011; Drouard and Woollings, 2018, Kautz et al., 2021), amplified quasi-stationary waves (Teng et al., 2016; Kornhuber et al., 2017), amplified Rossby wave patternspackets (e.g., Fragkoulidis et al., 2018; Kornhuber et al., 2020), and recurrent Rossby wave patternspackets (Röthlisberger et al., 2019). Fragkoulidis et al. (2018) showed that amplified Rossby waves are correlated with surface temperature extremes over NH and used process-based understanding to establish further association for the 2003 and 2010 NH heatwaves.

RRWPs can be considered as a subset of amplified Rossby waves with a condition that the transient eddies recur spatially in the same phase on a short time scale of days to weeks. Here, we focus on recurrent Rossby wave patternsRRWPs are closely related with blocking. RRWPs forming upstream of a block can sustain the block (e.g., Shutts, 1983; Hoskins et al., 1985; Hoskin and Sardeshmukh, 1987). RRWPs can also form downstream of blocks because of the near constant phase of the wave breaking (trough) on the downstream flank of the blocks (Barton et al., 2016; Röthlisberger et al., 2018). Here, we focus on recurrent Rossby wave packets to explore their importance for heatwaves in south-eastern Australia (SEA).
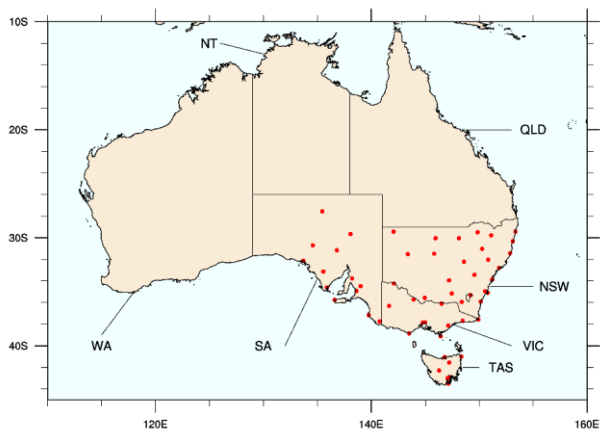
Figure 1. Map of Australia showing the states of South-eastern Australia (SEA): South Australia (SA), Tasmania (TAS), Victoria (VIC), and New South Wales (NSW). Other states shown are Queensland (QLD), Northern Territory (NT), and Western Australia (WA). Red dots indicate Australian Bureau of Meteorology's (BoM) monitoring stations used in this study (see Methods).

Broadly, heatwaves in SEA (Fig. 1), comprising the states of Victoria (VIC), New South Wales (NSW), South Australia (SA), and Tasmania (TAS), are associated with slow-moving transient anticyclonic upper-level potential vorticity (PV) anomalies over the Tasman Sea (e.g., Marshall et al., 2013; Parker et al., 2014a; Quinting and Reeder, 2017; Parker et al., ~~2019~~2020). The anticyclonic PV anomalies and the associated subsidence drive heatwaves over VIC (Parker et al., 2014b; Quinting and Reeder, 2017). These anticyclonic PV anomalies can form as ~~a~~ part of a synoptic-scale Rossby wave packet (RWP) (King and Reeder, 2021). These RWPs are often initiated several days before the onset of the heatwaves, but they amplify, and eventually break ~~over SEA as anticyclonic equatorward (LC1-type) Rossby wave breaking~~anticyclonically over SEA (Parker et al., 2014a; O'Brien and Reeder, 2017).

Surface temperature anomalies associated with transient RWPs form, amplify, and decay on synoptic ~~timescales~~time scales, but the recurrence of RWPs in the same phase on a sub-seasonal ~~timescale~~time scale can result in persistent surface weather conditions by repeatedly re-enforcing the surface temperature anomalies (e.g; Hoskins and Sardeshmukh, 1987; Davies, 2015). Röthlisberger et al. (2019) termed this phenomenon "Recurrent Rossby wave packets" (RRWPs) and demonstrated a

3

statistically significant connection between RRWPs and the ~~persistent~~persistence of surface temperature anomalies in the Northern Hemisphere (NH). Ali et al. (2021) found that RRWPs are also associated with increased persistence of dry and wet spells in several regions across the globe.

~~However, at least for~~For some impacts, it is not only the simple occurrence of an extreme, however one defines an extreme, but also the duration of the extreme event that is important. This study addresses that aspect for the hot temperature extremes in the SH. More precisely, we evaluate the hypothesis whether an increase in R-metric, a measure of RRWPs (Röthlisberger et al. 2019), is associated with an increase in hot spell duration of the surface-temperature extremes over SH. Furthermore, we show how SH RRWPs relate to the persistent and extreme SEA heatwaves and demonstrate their association with RRWPs and atmospheric blocking the help of two case studies for the 2004 and 2009 heatwaves.

2. Methods

2.1 Data

This study uses ERA-Interim (ERA-I) reanalysis data (Dee et al., 2011) provided by the European Centre for Medium-Range Weather Forecasts on a 1° × 1° spatial grid and 6-hourly temporal resolution for 1979–2018. ~~Various fields are~~The datasets used ~~including horizontal velocity,~~ are meridional wind velocity, 2 m temperature~~,~~ (T2m), and PV~~, and sea surface~~. Daily maximum 2 m temperature ~~(SST).~~is derived from T2m data and the anomalies in daily maximum T2m data is calculated with respect to day of year mean for the period 1979–2018. The datasets are freely available to download from https://apps.ecmwf.int/datasets/data/interim-full-daily/levtype=pl/. ~~The~~ PV fields ~~in~~are used as it is for calculating the ~~SH~~blocking fields. However, for rest of the analysis, the PV fields are multiplied by ~~a factor of~~ -1. ~~The climatological mean is calculated with respect~~minus one, which implies that negative (positive) PV anomalies represent anticyclones (cyclones) similar to the ~~period 1980–2010~~NH.

2.~~1~~2 Recurrent Rossby Waves

85   The metric R, developed by Röthlisberger et al. (2019), is used ~~identify~~ to quantify the recurrence of synoptic-scale Rossby

wave ~~patterns~~packets. For the SH, we use the same R-metric data as in Ali et al. (2021). First, ~~a 14.25 day running mean of~~

~~6-hourly~~ meridional ~~velocity fields ($\hat{v}_{tf}(\lambda,t)$),~~ winds at 250 hPa are averaged between 35° S and 65° S, ~~are~~

~~calculated~~$v_{ma}(\lambda,t)$. To the resulting longitude-time data $v_{ma}(\lambda,t)$, a 14.25 day running mean is applied to isolate signals

with ~~timescales~~time scales longer than the synoptic ~~timescale for each longitude λ and time t.~~time scale. This results in a

90   longitude-time field of temporally smoothed, meridionally averaged 250 hPa meridional wind $v_{tf}(\lambda,t)$. The envelope of the

synoptic wavenumber contribution to the time-filtered ~~v~~$v_{tf}(\lambda,t)$ is extracted following Zimin et al., (2003)~~. To do this, the~~

~~time filtered v fields are~~) as follows: The $v_{tf}(\lambda,t)$ is transformed into the frequency domain for each t using a fast Fourier

transform over longitude, ~~$\hat{v}_{tf}$~~yielding Fourier coefficients $\hat{v}_{tf}(k,t)$~~,~~ for zonal wavenumber k at the time step t. Finally, an

inverse Fourier transform is applied to calculate the envelope of the wave while only considering contributions from a

95   selected band of synoptic wavenumbers $k=$$k = 4$–15. Thus, $R(\lambda,t)$ for each longitude λ and time t is calculated as

$$R(\lambda,t) = \left| 2 \sum_{k=4}^{k=15} \hat{v}_{tf}(k,t) e^{2\pi i k l_\lambda / N} \right| \tag{1}$$

where k is the wavenumber, l_λ denotes the longitudinal grid point index for longitude λ and $N = 360$ denotes the number of longitudinal grid points.

In most cases, large values of R reliably identify situations in which amplified waves (of distinct wave packets) recur in the

100   same phase. However, the definition of R does not contain criterion for recurrence of distinct wave packets. Thus, in a few

cases, high values of R over a few days may result from stationary synoptic-scale troughs or ridges (see Röthlisberger et al.

2019 for discussion on the metric R). Fig. A1 shows day-of-year climatology of the R metric in the Southern Hemisphere and

compares it to that of the Northern Hemisphere. The code for calculating R metric is freely available (~~check~~see Code and

data availability section).

105   ~~Phase and~~ For the phase amplitude information ~~of a particular wavenumber k can also be~~ used in Section 3.3, it is extracted

using the ~~same technique~~Fourier decomposition along the longitude of meridionally-averaged (35° S and 65° S) 250 hPa

meridian wind $v_{ma}(\lambda, t)$ as ~~in (1) and presented by Zimin et al. (2003).~~ used for calculating the metric R above. After applying the ~~inverse~~fast Fourier transform, ~~a complex number of~~ one obtains Fourier coefficients in the form $a + ib$ ~~is obtained. For extracting the wave packet or envelop, the amplitude of the complex number is taken as shown in (1). Instead of that, plotting~~ of complex numbers $\hat{v}(k, t)$. Plotting the complex number on a complex ~~plain~~plane provides information on the phase and amplitude at a given time step t for a particular wavenumber k. ~~This is used to obtain a phase amplitude distribution shown later.~~

2.2 Atmospheric blocks

~~Atmospheric blocks are identified from persistent anticyclonic PV anomalies averaged between 500 hPa and 150 hPa vertical levels with the detection scheme described in~~ Atmospheric blocking data is computed following the methodology of Schwierz et al. (2004) ~~as updated by Rohrer et al. (2018). The code used is available on GitHub (https://github.com/marco-rohrer/TM2D). The detection scheme uses a 1.3 PVU threshold, a persistence criterion of 5 days, and a minimum overlap of 0.7 between two timesteps. Blocking fields identified with this algorithm are available at 6 hourly temporal resolution and 1° × 1° spatial resolution. We tested the sensitivity of the blocking fields with a 1.0 PVU threshold for the two case studies and did not find blocking directly over SEA.~~

as in Rohrer et al. (2020) and Lenggenhager and Martius (2019). The detection scheme identifies persistent anticyclonic PV anomalies vertically averaged (VAPV) between 500 hPa and 150 hPa vertical levels. First, the VAPV anomaly is computed from the 30-day running mean climatology of the corresponding time step of the year for the years 1979–2018. An additional 2-day running mean filter is applied to smooth out high frequency transients. Then the algorithm identifies areas with VAPV $\geq$ 1.3 PVU in the SH. The identified areas having a persistence criterion of 5 days, and a minimum overlap of 0.7 between consecutive time steps are classified as blocks. Blocking fields identified with this algorithm are available at 6 hourly temporal resolution and 1° × 1° spatial resolution. We tested the blocking fields with a less stringent threshold of VAPV $\geq$ 1.0 PVU for the two case studies and did not find blocking directly over SEA. The code used to calculate blocks is available on GitHub (See Code and data availability).

2.3 South-eastern Australian Heatwaves

A station-based ~~heatwave~~temperature dataset is used to ~~focus on~~identify extreme and persistent heatwaves in SEA ~~to study the links between RRWPs, blocks, and QRA conditions~~. Following the methods developed in Parker et al. (2014a) and refined in Quinting and Reeder (2017), heatwaves in SEA in December–February (DJF) are detected from temperatures observed at the Australian Bureau of Meteorology's (BoM) monitoring stations (Fig. 1). The BoM's Australian Climate Observations Reference Network – Surface Air Temperature (ACORN-SAT, available at _http://www.bom.gov.au/climate/data/acorn-sat/#tabs=ACORN%E2%80%90SAT_) is a high-quality temperature dataset used to monitor long-term temperature trends~~.~~ from 112 weather stations across Australia. The dataset provides a daily maximum temperature (TMAX) for each station. These TMAXs are extracted for stations in SEA as defined here~~,~~ for DJF from 1979 to ~~2019~~2018. The 90th percentile TMAX (T90) is then calculated for each station for each month in DJF. A _heatwave_ is defined as any period of at least four consecutive days for which the TMAXs at three or more ~~of these~~ stations equal or exceed the T90 for that station and month. From here on, the term "_heatwave_" refers to the heatwave in SEA. This criterion results in 57 heatwaves, ~~which were~~ on ~~an~~ average 8 days long, with the ~~longest~~most prolonged heatwave lasting 22 days~~.~~ starting in December 1990. Note that the ~~purpose of the~~ heatwave identification scheme ~~is~~aims to identify the most intense and ~~most~~ persistent heatwaves in SEA, and thus serves a different purpose than the hot spell identification scheme described in the next section. Following Parker et al. 2014a, a day that is part of the SEA heatwaves is termed as SEA heat day~~.~~ (SEA HD). For evaluating the co-occurrence of SEA HD with RRWP conditions, high R_{SEA} days are defined as days exceeding the 90th percentile of the daily mean R averaged over the longitudinal extent of SEA (between 130° E and 153° E). The 90th percentile threshold is a subjectively chosen threshold consistent with the threshold for TMAX. ~~Sensitivity~~A sensitivity test with a threshold of 85th percentile did not change the conditional probability ~~shown~~reported in section 3.3 and table C1.

2.4 Hot Spells in the SH

Figure 2: (a) Total number of hot spells in November–April identified at each grid point between 20° S and 70° S. (b) The 95th percentile of hot spell durations in days.

Hot spells are identified for all SH grid points between 20°S and 70°S for 1980–2016 using 2 metre temperatures (T2M)

155 from the ERA-I fields at 6 hourly temporal resolution and 1-degree spatial resolution. The hot spells definition follows that

of Röthlisberger et al. (2019), in which a hot spell is calculated for each grid point as consecutive values exceeding the 85th

percentile from the linearly detrended T2M fields. Spells separated by less than a day are merged to form a single

uninterrupted spell. Spell durations of less than 36 hours are excluded from further analysis. Contrary to the SEA heatwave

identification scheme, the purpose of the hot spell identification scheme isaims to identify many (warm periods that are not

160 necessarily overly extreme) warm periods at each grid point, which can then be used for statistical analyses of the factors

that determine the duration of these events. This statistical analysis (see next section) will be used to quantify the effect of

RRWPs on the persistence of warmhot surface weather. To ensure a large sample size for robust statistical results, we

identify hot spells for the period of November to April. Figure 2a shows the spatial distribution of the number of hot spells at

each grid point between 20° S and 70° S. Higher number ofOver land, many hot spells are seen over land where parts of

165 SEA, South Africa, and South America ~~show~~, having 350 or more spells. The 95th percentile for hot spell duration varies

from 6 days to more than 2 weeks (Fig. 2b). Over SEA, the 95th percentile duration varies from a week to roughly 2 weeks.

2.5 Weibull regression model to assess the effect of RRWPs in the SH hot spells

To quantify the effect of RRWPs on the persistence of hot surface weather, we extend an analysis from Röthlisberger et al.

(2019) to the SH, including SEA, using the same statistical model setup, a Weibull regression model. This model allows us

170 to model the distribution of the duration of hot spells at each grid point. An advantage of Röthlisberger et al.'s (2019) model

is that we do not need to subjectively define the duration of a "significant" spell because the model ~~accounts for~~quantifies the

~~assessment of~~ changes in all quantiles of the spell duration modelled. The null hypothesis tested here at each grid point is

that RRWPs have no effect on the duration of hot spells~~, which is tested~~ at ~~each~~the respective grid point. The Weibull model

is only briefly introduced here. Please refer to Röthlisberger et al. (2019) for further details and their Supporting Information

175 for a detailed introduction to the Weibull model.

To fit the Weibull model to the observed spell duration distribution, a representative value of the R-metric needs to be

assigned to each hot spell. This is achieved in the following way: for each hot spell i at grid point g with a duration $D_{g,i}$, the

raw R metric $R(\lambda, t)$ is longitudinally averaged within a 60° longitudinal sector centred at the grid point g with longitude λ_g

to yield $R_{lon}(\lambda, t)$. Then, a median of $R_{lon}(\lambda, t)$ is calculated for the lifetime of the hot spell to assign a representative value

180 of R ($\tilde{R}_{\lambda_g,i}$) for each spell. ~~Thus, our~~The model is ~~given~~formulated as:

$$\ln(D_{g,i}) = \alpha_{0,g} + \alpha_{1,g}\tilde{R}_{\lambda_g,i} + \sum_{j=2}^{6} \alpha_{j,g}m_j(t_{g,i}^{start}) + \sigma_g\epsilon_{g,i} \quad ; i = 1, \dots n_g. \tag{2}$$

~~Hereby~~Here, $\alpha_{0,g}$ is the intercept, $\alpha_{1,g}$ is the regression coefficient for $\tilde{R}_{\lambda_g}$ and the $\alpha_{j,g}, j = 2, \dots, 6$ are regression

coefficients for dummy variables $m_j(t_{g,i}^{start})$ that take the value 1 if spell i starts in month m_j, and zero otherwise. The

coefficients $\alpha_{j,g}$, therefore, account for possible seasonality in the spell duration distribution at grid point g (e.g., longer hot

185 spells in May compared to, e.g., September), while σ_g is a scale parameter and the $\epsilon_{g,i}$ are error terms. ~~The~~

~~quantity~~Exponentiated regression coefficients, e.g., $\exp(\alpha_1)$ ~~is~~are usually referred to as acceleration factor (AF~~)~~). The

$\exp(\alpha_1)$ and is of particular interest here, as it quantifies the factor of change in all quantiles of the distribution of spell

9

duration <u>distribution</u> at grid point g per unit increase in $\tilde{R}$ (Hosmer et al., 2008; Zhang, 2016; Röthlisberger et al., 2019). An $AF > 1$ implies an increase in all spell duration quantiles with increasing $\tilde{R}$ (i.e., during RRWPs), and conversely for an AF

190 < 1.

Furthermore, fitting the model (2) to spell durations at all grid points ~~thus~~ results in a spatial field of AF. The statistical significance of the AF values is evaluated in a two-step approach. First, a p-value for the above null hypothesis is computed exactly as in Zhang (2016). Then, the false-discovery-rate (FDR) test of Benjamini and Hochberg, (1995) is applied to the resulting field of p-values. The FDR test controls for type I errors, i.e., falsely rejecting <u>the</u> null hypothesis that can occur

195 substantially in analyses like this one where multiple tests are being performed independently from each other at each grid point (e.g., Wilks 2016). Here we follow the recommendation of Wilks (2016) and allow for a maximum false-discovery-rate α_{FDR} of 0.1.

~~This model is fitted to durations of hot spells at each grid point. It results in a spatial field of regression coefficients $\alpha_{j,g}, j =$~~

~~$0, ..., 6$, together with their p values. Here, $\alpha_{1,g}$ represents the effect of $\tilde{R}$ on the hot spell duration. The $\exp(\alpha_1)$, referred to~~

200 ~~as the acceleration factor (AF), corresponds to the factor of change in all quantiles of the spell duration D per unit increase in~~

~~$\tilde{R}$ (Hosmer et al., 2008; Röthlisberger et al., 2019; Zhang, 2016). Statistical significance of AF is evaluated after controlling~~

~~the false-discovery rate (FDR) (Benjamini and Hochberg, 1995) for type I errors due to falsely rejecting null hypothesis in~~

~~multiple independent tests by setting the FDR threshold, α_{FDR} to 0.1 as recommended by Wilk's (2016). Thus, regions with~~

~~$AF > 1$ ($AF < 1$) experience an increase (decrease) in spell duration with increasing (decreasing) R.~~

205 **3. Results**

3.1 RRWPs and hot spell durations

10
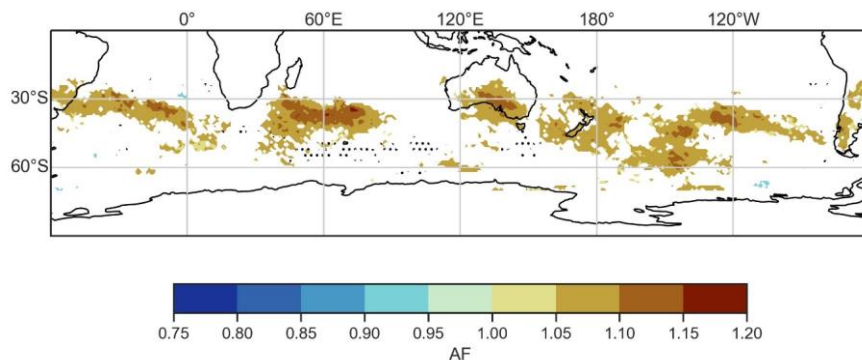
Figure 3: Statistically significant acceleration factors (AF) for hot spells in November–April between 20° S and 70° S. Colours show AFs from a Weibull model with R metric as a covariate. Stippling indicates grid points where spell durations do not follow the Weibull model based on the Anderson–Darling test at a significance level of 0.01.

210 The Weibull analysis reveals that RRWPs are significantly correlated with the duration of hot spells in several regions within

the SH and including over SEA (Fig. 3). Recall that *AF* larger than 1 means that an increase in ~~RR~~R is related to an increase in

hot spell duration and conversely for *AF* smaller than 1. Thus, several parts of central and southern Australia, including the

states of SA, VIC, NSW, and TAS, experience longer hot spells during periods when RRWPs occur. Northern Australia,

however, does not show such a correlation with RRWPs, which agrees with previous studies showing different dynamical

215 pathways for Northern and Southern Australian heatwaves (Risbey et al., ~~2017~~2018; Quinting and Reeder, 2017; Parker et

al., ~~2019~~2020). Other statistically significant areas over land include parts of South America: southern Brazil, Bolivia, and

parts of Argentina and Chile. For Northern Hemisphere summer half-year, the significant AFs, larger than 1, form a

wavenumber 7 pattern (Röthlisberger et al., 2019). In contrast, no clear wave pattern emerges for the SH in the significant

AFs in Fig. 3. The difference in *AF* patterns between the two hemispheres is consistent with different climatological

220 stationary wave patterns. The spatial pattern in Figure 3 highlights areas where the transient waves building up the RRWPs

have a predominant phasing in summer. In summary, the regression analysis shows that RRWPs are significantly associated

with the duration of hot spells in several SH regions over land, including SEA. However, the Weibull analysis does not

provide any information about the processes and hence potential causal link between RRWPs and the most intense SEA

heatwaves. Accordingly, we next focus on SEA heatwaves and elucidate the role of RRWPs and blocks for two selected

225 cases studies of SEA heatwaves and investigate further co-occurrence of SEA heatwaves and days with high *R* ~~activity~~.

3.2 RRWPs, and Blocks. and QRA during two extreme and persistent SEA heatwaves

3.2.1 Case 1: 2004 Heatwave

The February 2004 heatwave (7–22 February) lasted for 16 days. More than 60% of continental Australia recorded

temperatures above 39°C during this event (National Climate Centre, 2004). At the time, this event was the most severe

230 February heatwave on record in both spatial and temporal extent and ranked in the top five Australian heatwaves for any

month (National Climate Centre, 2004). More than 100 stations in SA, NSW, and northern VIC experienced record

temperatures for February, and in some regions all-time records were set for consecutive days of heat (BoM, 2004). Previous

studies have shown that the upper-level anticyclonic PV anomalies over SEA during the heatwaves are associated with

subsidence and is the major process causing the high surface temperature anomalies (e.g., Quinting and Reeder, 2017; Parker

235 et al., ~~2019~~2020). The surface flow associated with anticyclonic anomalies may also advect warm continental air due to the

north westerly flow at lower levels (e.g., Parker et. al. 2014b). The warm advection associated with the surface flow can be

significant even with weak upper or lower-level winds. Here, we show how RRWPs contribute to persistent anticyclonic PV
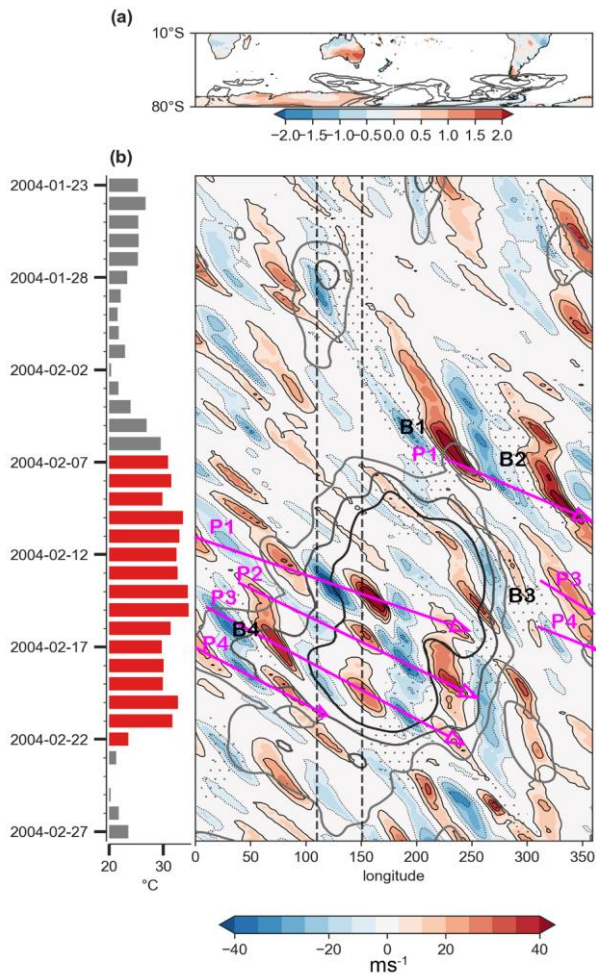
anomalies over SEA.

12
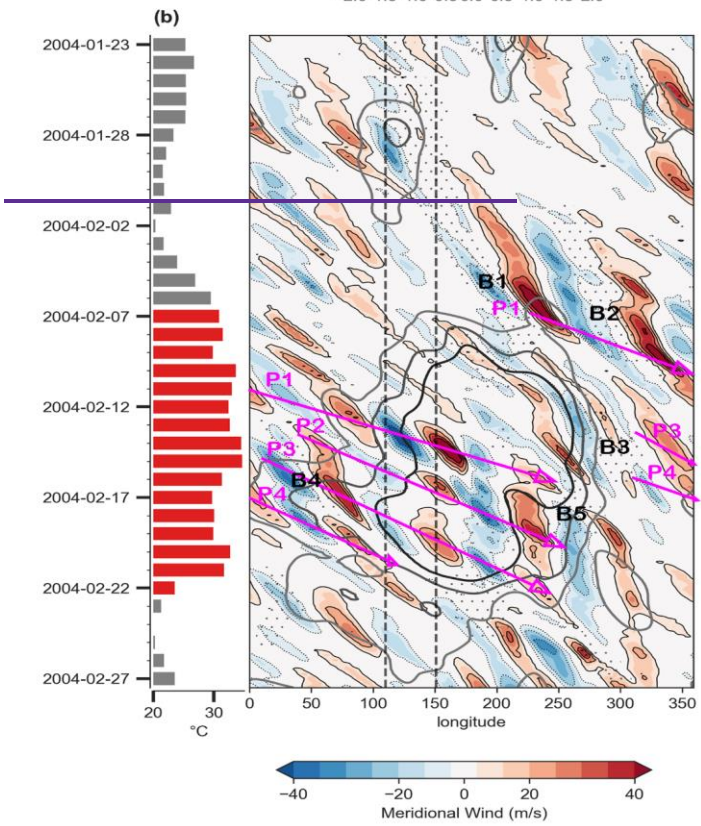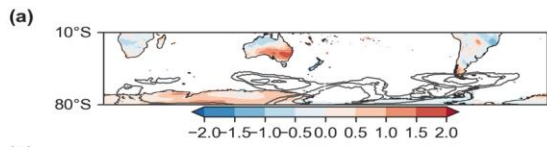
Figure 4: RRWPs, and blocks during 2004 SEA heatwave. (a) Filled contours depict the time-mean of the standardized day of year anomalies of daily maximum 2 m temperatureT2m over land for the duration of the heatwave. Contours show the mean blocking frequency during the heatwave (5, 10, 20 %). (b) Bars show daily maximum 2 m temperature averaged over SEA (°C); red marks the heatwave period. The Hovmöller diagram shows the meridional wind at 250 hPa averaged between 35° S and 65 °S (filled contours, m/sms⁻¹), R values (grey contours, 6, 8, 10 m/sms⁻¹), and longitudes at which at least one grid point between 40° S and 70° S featured an atmospheric block (stippling). Rossby wave packets (blocks) are labelled in magenta (black).
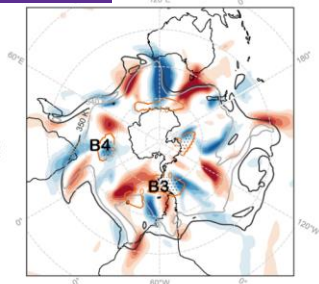
14

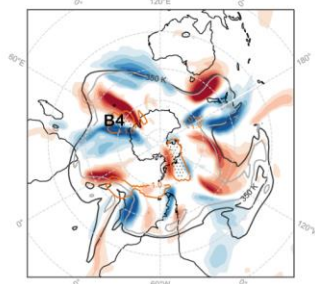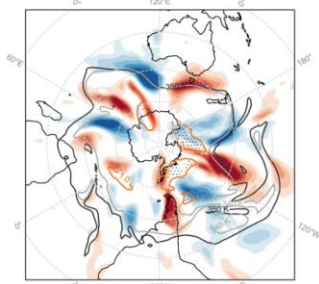(a) 2004-01-26 12:00
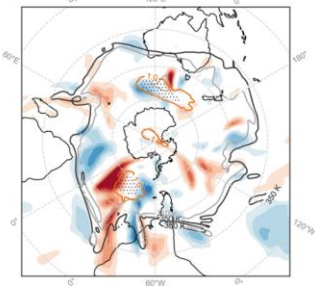
(b) 2004-02-05 12:00
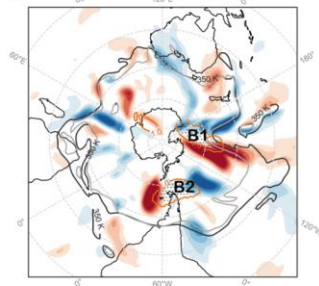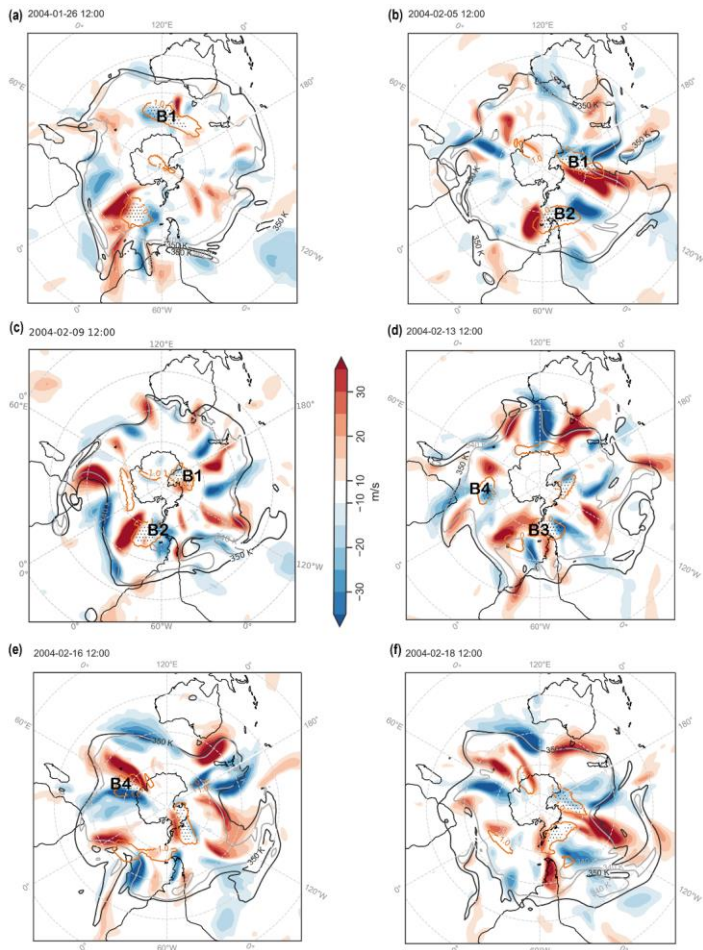
(c) 2004-02-09 12:00
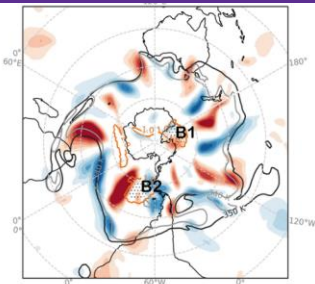
(d) 2004-02-13 12:00

(e) 2004-02-16 12:00

(f) 2004-02-18 12:00

15

Figure 5: (a), (b), (c), (d), (e), and (f) show meridional velocity at 250 hPa (colour shading), 2 PVU contours at isentropes 340 K (blackgrey line) and 350 K (greyblack line) at various time steps. Stippling and orange contours show blocks identified using a 1.3 and 1.0 PVU threshold, respectively.

Figure 4 shows the flow conditions prior to and during the heatwave (Fig. 4b) and the corresponding T2m anomalies over

255   SEA (Fig 4a.). The Hovmöller diagram (Fig. 4b) shows the 35° S and 65° S averaged meridional wind. Figure 5 shows the

upper-level flow at different time steps prior to and during the heatwave. We use the two figures (Fig. 4 and Fig. 5) to

demonstrate the role of transient RWPs and blocks during the heatwave and present that next.

During this event, several Rossby wave packets were observed, recurrently amplifying in the same phase forming a ridge

over SEA. The upper-level flow over SEA was zonal prior to the heatwave (Fig. 5a). An upper-level ridge forms over SEA

260   around 5 February prior to the heatwave (Fig. 5b). The flow becomes more amplified in the subsequent days with a

circumglobal amplified wave pattern apparent around 9 February (Fig. 5c). The amplified wave, part of a transient and

nonstationary Rossby wave packet, RWP (P1 in Fig. 4b), arrived over the southern Indian Ocean, and an upper-level ridge

began to form over Australia which amplified further around 13 February (Fig~~. 5e~~. 5d). Two further ridges formed over SEA

on 16 and 18 February (Fig. 5e, 5f), each ridge being part of a transient nonstationary RWP initiated upstream of Australia

265   (P3, P4 in Fig ~~5b~~4b). These series of upper-level recurrent ridges were part of the RRWPs and contributed to the persistence

of the heatwave. These recurrent ridges associated with RRWPs were also detected by the metric R (grey contours in Fig.

4b).

No blocks were identified directly over SEA during the heatwave, but blocks were present south of SEA and further

downstream (Fig. 4, 5). The RWP labelled as P1 in Figure ~~5b~~4b formed downstream of a block B1 ~~downstream of~~

270   ~~Australia~~in the Pacific Ocean (roughly 200° E), where the block moved from south of Australia a few days earlier (Fig.

~~5b~~5a). Another block B2 was simultaneously present in the vicinity of South America around 7 February~~.~~ (Fig. 4b). In the

next few days, simultaneous wave breaking was observed in the central Pacific Ocean and south of Africa in the Indian

Ocean. Another set of RWPs (P3 and P4 in Fig. 4b) ~~seems to have been set off by~~were associated with a block over the

Pacific Ocean (B3 in Fig. ~~5b~~4b, 5d). Simultaneously, another block was present south of South ~~America~~Africa (B4 in Fig.

275   ~~4b, 5d), and seem to initiate another RWP (P3 in Fig.~~ 4b, 5d). Block B4 was also associated with amplified Rossby waves

downstream over the Indian Ocean on 16 February (Fig. ~~5d~~5e). Thus, we argue that blocks could have played a key role in

the initiating, phasing, and meridional amplification of the ~~three~~four Rossby wave packets (P1–P4) that reached Australia

between 13 and 18 February. In summary, we saw recurring RWPs that passed over Australia during this period (Fig. 4b).

17

These waves were not stationary, they were not triggered in the same area, and not over Australia, and were initially not in phase upstream of Australia.

3.2.2 Case 2: 2009 Heatwave

The 2009 heatwave (27 January–9 February), although extensively covered in literature (e.g., Engel et al. 2013, Parker et al. 2014b), has been chosen because it is one of the most severe heatwaves in SEA. It lasted for 14 days. Between 28–31 January and 6–8 February, temperatures in SEA were exceptionally high. On Black Saturday, 7 February, the hot, dry, and windy conditions ~~worsened~~fuelled many catastrophic fires in VIC, which recorded 173 fatalities, and more than 2133 houses were destroyed (Karoly 2009; Parker et al., 2014b; VBRC 2010). During this heatwave, an anticyclone over SEA and the associated north-westerly flow at the surface advected hot continental air into SEA leading to extreme surface temperatures (Parker et al., 2014b). As for the 2004 Case, we next present the Hovmöller diagram (Fig. 6) and snapshots of upper-level flow (Fig. 7) to demonstrate the role of transient RWPs and blocks during the heatwaves.

Prior to the onset of the heatwave, the flow was already amplified with a wave breaking over SEA (Fig. 7a). Several ~~RRWPs~~RWPs were observed prior to and during this event (P1 and P2 in Fig. 6b). The ~~RRWPs~~RWPs prior to the heatwave were not in the same phase as those during the heatwave (Fig. ~~6b).~~6b), which is why the value of R-metric is not high around 25 January. Around 26 January, a Rossby wave packet (P2 in Fig 6b) was observed forming an upper-level ridge ~~forming~~ over Australia (Fig. 6b, 7b). In the subsequent days, the amplified wave broke anticyclonically over SEA (Fig. 7c), resulting in an anticyclonic PV anomaly over SEA (see Parker et al., 2014 for a detailed analysis of this event). On 2 February, a new ridge started forming over southern Australia (Fig. ~~7c~~7d) as part of Rossby wave packet (P3 in Fig 6b) and reached over SEA on 5 February (Fig. ~~7d~~7e). However, the upper-level ridge was transient and was replaced by another ridge around 7 February as part of another amplified wave (P4 in Fig. 6, Fig. ~~7e~~7f).

No blocks were identified directly over SEA during the heatwave (Fig. 6, 7). However, blocks were frequent upstream of SEA from 50° E to 70° E in the Indian Ocean (B2 in Fig. 6b, Fig. 7), and downstream of SEA from 200° E to 250° E (B1 in Fig. 6b, 7). Block B2 over the Indian ocean was particularly persistent and interacted with several amplified Rossby wave packets (~~T2, T4~~P2, P4). B2 began to weaken around 2 February (Fig. ~~7c~~7d) but restrengthened again on 5 February (Fig.

8d7e) due to injectionabsorption of low PV from a smaller southward moving block in the Indian Ocean (not shown). Therefore, B2 remained persistent throughout the heatwave. Rossby wave packet P1 formed downstream of the block B1B0 over the Pacific Ocean prior to the heatwave (Fig 6b, 7a).

So far, we have investigated the association of RRWPs with duration of hot spells. We also presented two cases of extreme and persistent SEA heatwaves to show how RRWPs can lead to the formation or replenish the anticyclonic PV anomalies over SEA. Figure B1 shows another case of SEA heatwave associated with RRWPs. In the next section, we extend the analysis to a climatological period (1979–2018) and explore high R_{SEA} conditions for all the SEA heatwaves.
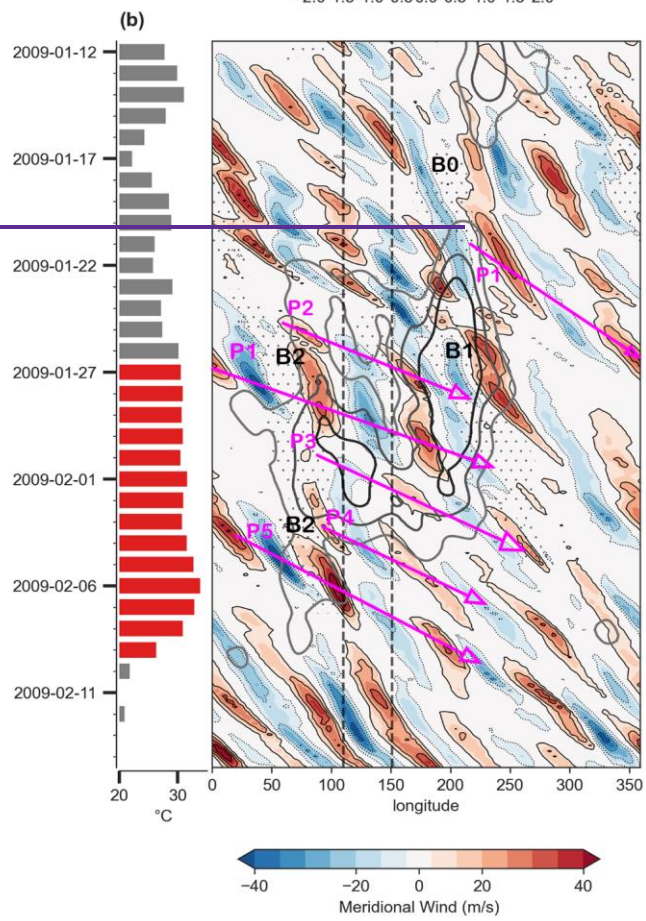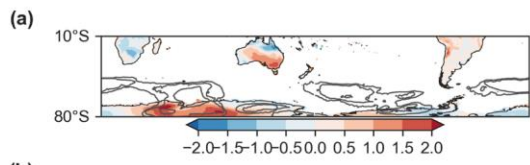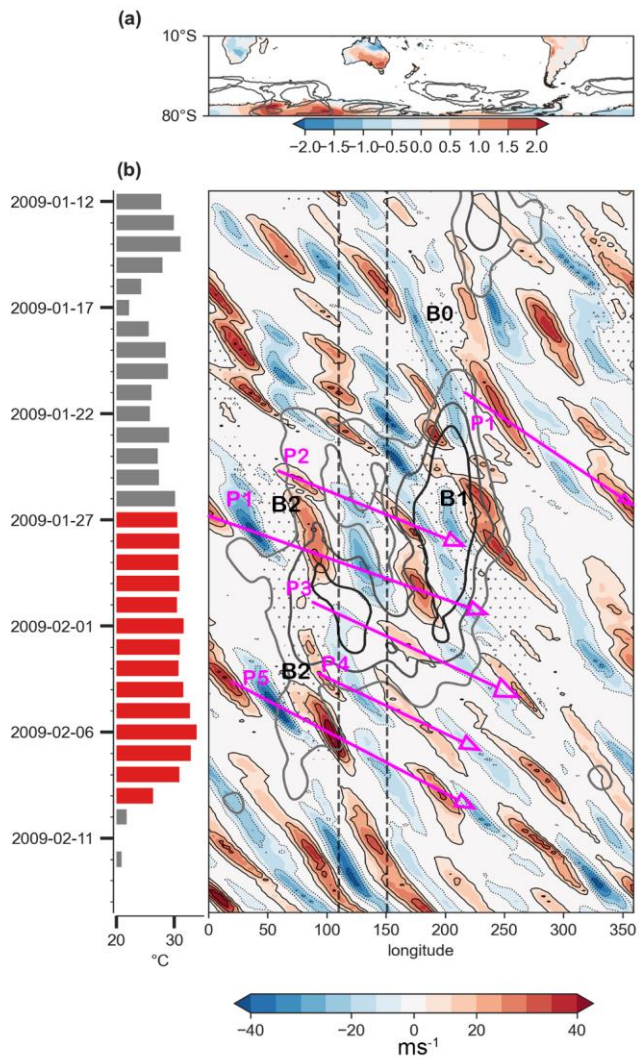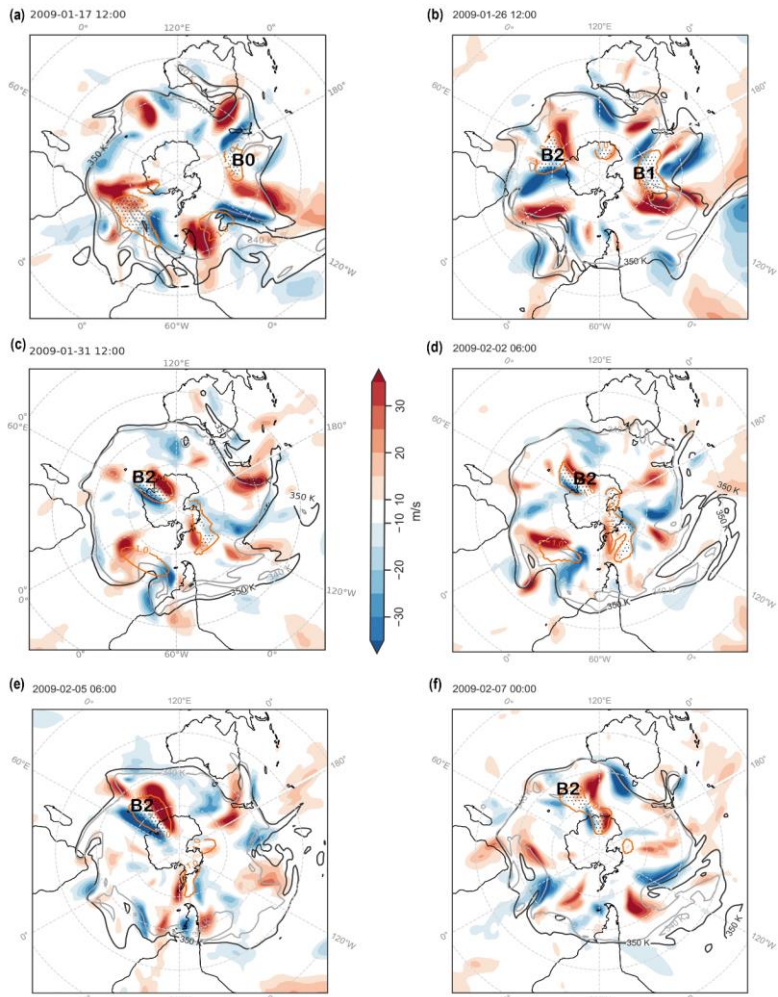
Figure 6: Same as in Fig. 4 but for February 2009 SEA heatwave.

Figure 7: Same as in Fig. 65 except for February 2009 SEA heatwave.

3.3 RRWP conditions during SEA heatwaves

First, ~~a~~we note ~~on~~ the co-occurrence of high R_{SEA} days and SEA heatwave days (SEA HD) as defined in section 2.3. Out of 352 days with high R_{SEA}, 67 co-occur with SEA HD, and 285 do not co-occur (Table C1). Thus, the conditional probability of a SEA HD given high R_{SEA} is 0.19 (67/352=0.19), which is higher than the climatology (457/3520=0.13). The conditional probability further increases to 0.34 on filtering out the high R_{SEA} days containing a cyclonic PV anomaly over SEA (Table C1). Many high R_{SEA} days do not co-occur with SEA HD, which ~~clearly~~ indicates that R is not a sufficient condition for SEA heatwaves on its own. We, therefore, further explore ~~that~~ why some high R_{SEA} days co-occur with SEA HD while others do not.

High R_{SEA} days co-occurring with SEA HD feature a large anticyclonic PV anomaly over SEA (Fig. 8a) on the 350 K isentropic surface. The 2 PVU isoline on the 350 K isentropic surface, indicating the dynamic tropopause, is also located over SEA, thereby indicating a suitable choice of the isentropic surface. Upstream and downstream of the anticyclonic PV anomaly over SEA feature cyclonic PV anomalies that are also located equatorward of the highest blocking frequencies (black contours in Fig. 8a). These may correspond to the cyclonic PV anomalies surrounding omega-type blocking or the cyclonic PV anomalies of the dipole blocks. Since blocking is a binary dataset, the blocking frequency in ~~Figures 8a and 8b~~Figure 8 indicates the percentage of days on which a grid point features a block. Thus, for high R_{SEA} days co-occurring with SEA HD, blocks are more frequent over the Indian and the south Pacific Oceans close to the Antarctic coast (Fig. 8a) compared to high R_{SEA} days without co-occurring SEA HD (Fig. ~~8a~~8b, 8c) and less frequent over the 60° S latitude, the latitudinal band featuring high blocking frequency in the DJF climatology (Fig. 8c, 8f).

In contrast, on high R_{SEA} days not co-occurring with SEA HD (Fig. 8b), there is no ~~spatial preference for the~~clear anticyclonic PV ~~anomalies~~anomaly over SEA. Weak zonally elongated PV anomalies are present over the ocean basins, that are co-located with the blocking frequency fields south of south Africa, and in the Indian and south Pacific oceans (black contours in Fig. 8b). ~~Near Australia, the centroid of the contour of anticyclonic PV anomaly appears around 30° downstream of SEA over New Zealand (Fig. 8b) compared to over SEA in Figure 8a.~~ The difference in the spatial distribution of PV anomalies on the high R_{SEA} days not co-occurring with SEA HD and the high R_{SEA} days co-occurring ~~on~~with SEA HD

23

340   suggests that only the RRWPs whose phase is conducive to forming ridges over SEA are important for SEA heatwaves.

Furthermore, Figure D1 shows the PV composite for all SEA HD.
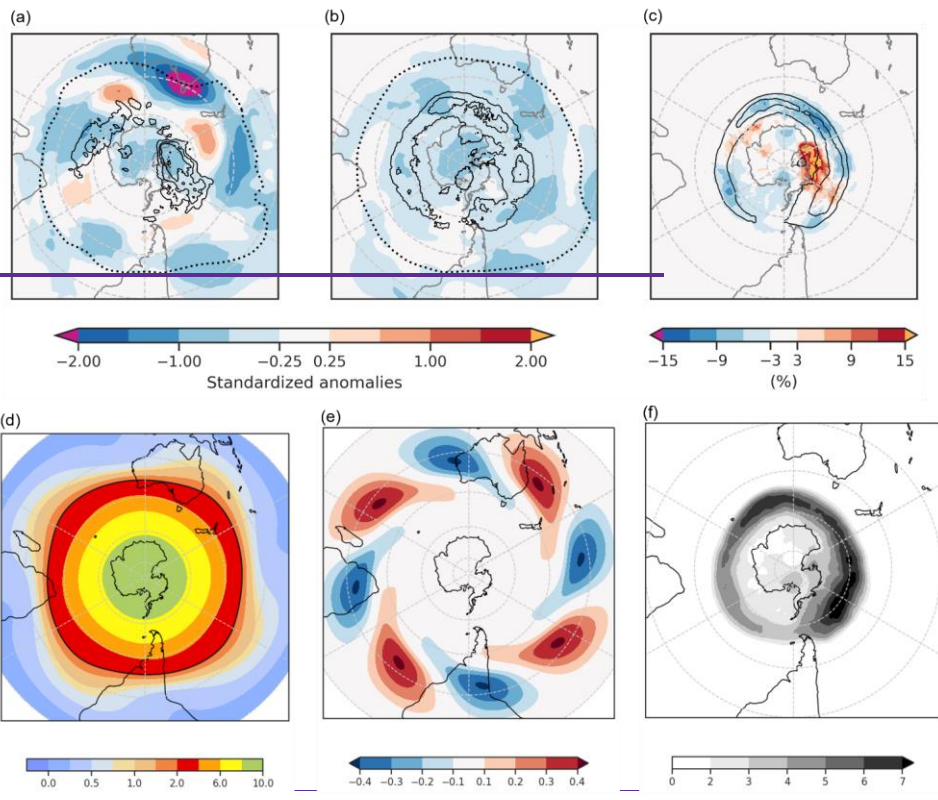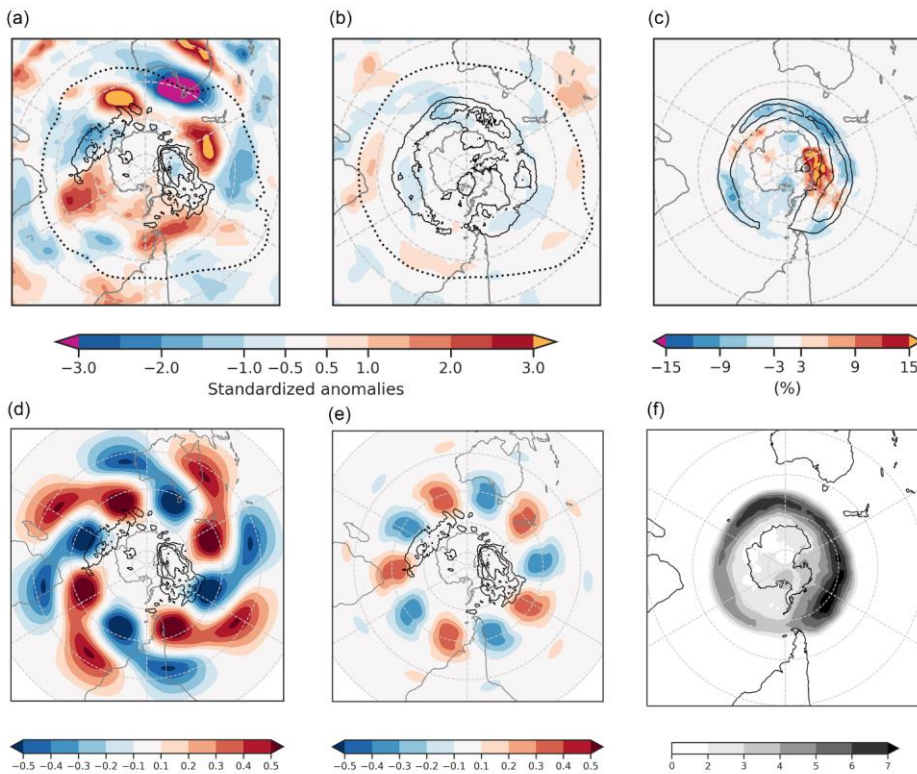
Figure 8: Standardized PV anomalies on the 350 K isentrope with respect to the DJF climatology (1979–2018) for (a) High R_{SEA} days and SEA heatwave days (HD), (b) High R_{SEA} days and non-SEA HD. Dotted black lines show 2 PVU contour in the mean PV fields for (a) and (b), and black contours show mean blocking frequency contours at 5, 10, 15 % for the same. (c) Shows the difference in blocking frequency between (a) and (b). (d) shows the ~~sum of~~ WN4 component for the mean PV (in PVU) ~~from the zonal wavenumber, *k* = 4 component of the DJF climatology at 350 K (shown~~ for High R_{SEA} and SEA HD in (a), (e) ~~and the k=0 (the DC)~~ shows WN5 component.~~,~~ for the same, and the black contours in (d) and (e) show the blocking frequency as in (a). (f) shows the climatological mean blocking frequency (%) for DJF, and black contours in (c) show the same at 4, 6 ~~%,~~ %.

26

(a) High R and SEA HD   (b) High R and non SEA HD
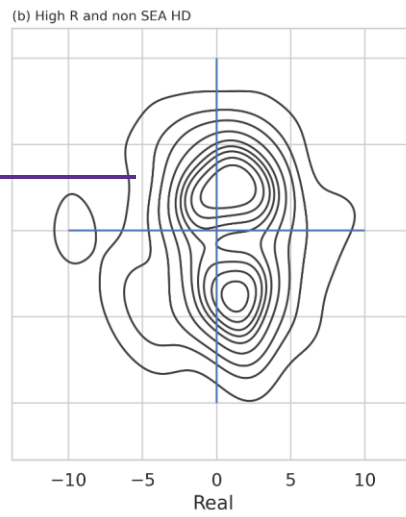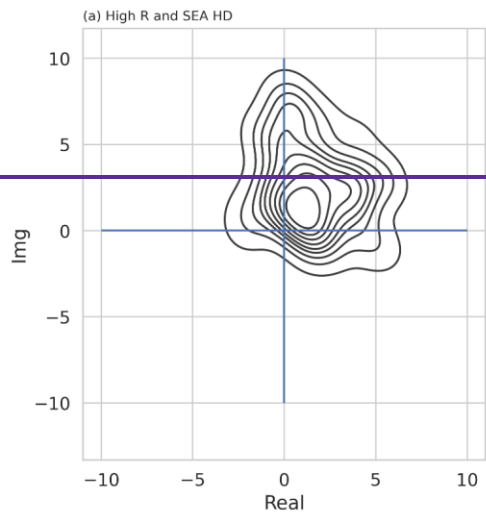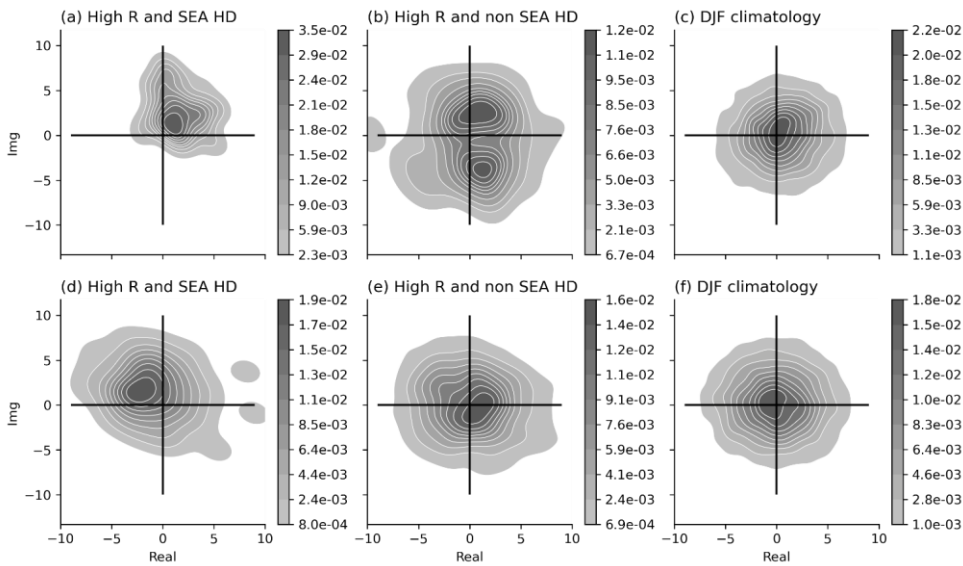
Figure 9. Bivariate kernel density estimate using Gaussian kernels in the complex ~~plain~~plane of the Fourier decomposed meridional wind at 250 hPa averaged between 35° S and 65° S. Only zonal ~~wavenumber 4 is~~WN4 (top) and WN5 (bottom) are shown for days belonging to (a, d) high R_{SEA} and SEA HD, ~~and~~ (b, e) high R_{SEA} and non-SEA HD~~.~~, and (c, f) DJF climatology.

In addition to the ridge over SEA, a circum-hemispheric zonal wavenumber (WN) 4 ~~(WN4)~~and 5 pattern is present in the composite mean PV fields for high R_{SEA} days co-occurring on SEA HD (Fig. ~~8a). This WN4 pattern does not have the same~~ ~~distribution of~~ 8a), where five distinct highs (negative PV anomalies ~~as the WN4 extracted from the Fourier decomposition~~ ~~of the climatological mean PV field for DJF: the WN4 climatology features~~) and four lows are visible in the 30° to 60° latitudinal band. We hypothesize that Rossby waves in a particular phase helps to establish the anticyclonic PV ~~anomaly~~ ~~node roughly 30° west of~~ anomalies over SEA (~~Fig 8d, 8e).~~

~~A high fraction of WN4 flow during high~~ in Fig. 8a). Hence, we present Fourier decomposition of the composite mean PV field for high R_{SEA} days co-occurring ~~on~~with SEA HD ~~is in phase (Fig. 9). Figure 9 shows the phase and amplitude density~~ ~~distribution of the WN4 component of the meridional winds averaged between 35° S and 65° S. Phase and amplitude~~ ~~information~~(Fig 8d, 8e). To check ~~for each wavenumber can be extracted using a Fourier decomposition as shown in section~~ ~~2.1. On high R and SEA HD, the density distribution in the complex plain is unimodal point to~~ a preferred phasing ~~of the~~

28

~~wave that is reflected~~during high R and SEA HD, we also present the phase-amplitude distribution of the meridionally-averaged meridional wind, v_{ma} later in ~~WN4 pattern visible in the PV composite~~ Figure 9.

The WN4 and WN5 components (Fig. 8a). ~~On~~8d, 8e) of the composite mean PV field for high R_{SEA} ~~and~~days co-occurring with SEA HD brings out the role of the phase of the waves in contributing to the anticyclonic anomalies over SEA in Figure 8a more clearly. Over SEA, both WN4 and WN5 components have the same phase and contribute to the anticyclonic PV anomalies. The northeast and southwest orientation in the WN4 pattern over Australia may be associated with the anticyclonic wave breaking over Australia. In the south Pacific and the Indian Oceans, we observe cyclonic PV upstream and downstream of the blocking frequency contours (Fig. 8d, 8e).

Figures 8d and 8e suggest that high R_{SEA} days that co-occur with SEA HD have a particular phase conducive to forming anticyclonic PV anomalies over SEA. Therefore, as stated earlier, we next present the phase-amplitude distribution for WN4 and WN5 components to test this hypothesis in Figure 9 for the latitudinally-averaged (35°S–65°S) daily meridional wind velocity at 250 hPa, v_{ma}. We compare the density distribution for days with high R_{SEA} and SEA HD with high R_{SEA} and non-SEA HD. Using a Fourier decomposition (see Methods), we extract the WN4 and WN5 components and plot the phase and amplitude density distribution on a complex plane using a Gaussian kernel density estimate (KDE). To determine the amount of smoothening, we used the default bandwidth estimation method, the Scott method. Since we are interested in the qualitative spread of the WN components (e.g., unimodal, bimodal) rather than quantitative estimation of the probability density function, the choice of our smoothening parameters for the KDE is sufficient.

On high R_{SEA} and SEA HD, the density distribution of the WN4 component in the complex ~~plain is bimodal and generally much~~plane is unimodal (Fig. 9a), which points to a preferred phase of the waves. From Fig. 8d, we know that it predominantly forms an anticyclonic PV anomaly over SEA. The density distribution of WN4 for high R_{SEA} and non-SEA HD has a broader~~, that agrees with the PV composite that shows no clear WN4 pattern (Fig. 8b). The phase distribution for wavenumber 4~~ bimodal spread. The distance from the origin of the complex plane represents the amplitude; hence, the peak of WN4 distribution of high R_{SEA} days have a higher amplitude (Figs. 9a, 9b) compared to the DJF climatology whose peak is almost centred at the origin (Fig. 9c). For WN5, the peak of the distribution for days with high R_{SEA} and SEA HD have a

different phase and higher amplitude compared to high R_{SEA} and non-SEA HD (Figs. 9c, 9d) and the DJF climatology (Fig. 9e).

395 The phase distribution for WN4 and WN5 is shown here because ~~it emerges~~they emerge as the dominant ~~pattern~~patterns in the composite mean (Fig. 8a), whereas the density distributions for other wavenumbers (k=3, 6, and 7) do not exhibit a clear difference between high R_{SEA} and SEA HD compared to high R_{SEA} and non-SEA HD and DJF climatology (not shown). Overall, our results agree with the understanding of SEA heatwaves featuring upper-level anticyclonic PV anomalies over SEA (Marshall et al., ~~2013~~2014; Parker et al., 2014b; Quinting and Reeder, 2017), and we show how RRWPs in a particular

400 phase (WN4 and WN5) are conducive to forming anticyclones over SEA.

4. Discussion

During the 2004 and 2009 SEA heatwaves, we find transient and fast-moving Rossby waves organized in wave packets, recurring in the same phase to form a ridge over SEA, thereby contributing to the persistence of the heatwave conditions. This persistence arises by recurrence, in contrast to the persistence arising from stationary weather features such as slow-

405 moving Rossby waves (e.g., Wolf et al., 2018) or blocking anticyclones (e.g., Kautz et al. 2022). The Rossby wave packets observed during the two SEA heatwaves were not always initiated in the same area. In the 2004 case, these waves were mostly not in phase upstream of Australia, whereas in the 2009 case, they were also in phase upstream over the Indian Ocean. Blocks were observed upstream and downstream during the two heatwaves ~~and~~which suggests that blocks could play a role in initiating the RWPs and/or in modulating their phase. Figure ~~D1~~E1 presents the relationship between R anomalies

410 and the blocks in the Indian and south Pacific Oceans for DJF. Overall, our results agree with Risbey et al. (2018) and King and Reeder (2021), who reported transient waves in the Indian Ocean preceding SEA heatwaves and transient circulation anomalies during SEA heatwaves. More specifically, we show how recurrent Rossby waves aid in the persistence of the well-known upper-level anticyclonic PV anomalies during SEA heatwaves by forming recurrent upper-level ridges.

The relevance of RRWPs for persistent SEA heatwaves documented in these two case studies is consistent with the results of

415 the Weibull regression analysis, which reveals a significant positive statistical link between the duration of hot spells over SEA and RRWPs. PV composite for high R_{SEA} days co-occurring with SEA heatwaves shows an anticyclonic PV anomaly

over SEA (Fig. 8), which is a typical feature of SEA heatwaves (Parker et al., 2014b; Quinting and Reeder, 2017). The PV composite also shows a wavenumberwavenumbers 4 and 5 pattern, where the anticyclonic PV anomalies are located upstream and downstream of blocking frequency maxima. Furthermore, the WN4 and WN5 components of the mean PV field (Figs. 8d, 8e) as well as the phase-amplitude distribution of the zonal wavenumber in the complex plainWN4 and WN5 components of the meridional wind velocity (Figs. 9 a, d) indicates a preferred phasing for high R_{SEA} days part of SEA heatwaves (Fig. 9).. The results from the Weibull regression analysis also suggests preferred phasing of the transient eddies not only over SEA but also upstream and downstream of it. Therefore, recurrent Rossby wave packets in the right phase could help to foster the anticyclonic anomalies over SEA for time periods exceeding the lifespan of an individual wave packet. Hence, the combined evidence from the literature summarized above, together with the observations from the two case studies and the results from the regression analysis, suggest a causal link between RRWPs and persistent SEA heatwaves. The proposed link works as follows: heatwaves over SEA are forced by subsidence occurring in anticyclones of SEA (e.g., Quinting and Reeder, 2017). RRWPs result in the repeated formation of these ridges over SEA and thereby contribute to the persistence of the ridges and thus, the heatwaves. However, not all SEA HD are associated with RRWPs, and hence other dynamical pathways for SEA heatwaves exist. In addition, local negative soil moisture anomalies strengthen positive temperature anomalies through increased surface sensible heat fluxes and may thereby extend the duration of heat wavesheatwaves (e.g., Green 1977; Seneviratne et al. 2010; Martius et al. 2021).

A reverse causal link between surface temperature anomalies during SEA heatwaves and R_{SEA} is theoretically possible, namely that the positive surface temperature anomaly contributes substantially to the upper-level ridge and that this ridge amplification increases R_{SEA}. This causal link cannot be distinguished in our Weibull model set-up. However, model experiments from Martius et al. (2021) suggest that the influence of surface temperature anomalies over Australia on the upper-level (250hPa250 hPa) geopotential height and wind anomalies is quite small; therefore, the imprint on R-metric after the latitudinal averaging is even smaller.

5. Conclusions

440   We find that RRWPs are associated with a significant increase in the persistence of hot spells in the SH. In several parts of

SEA, including the states of South Australia, New South Wales, Victoria, and Tasmania, longer hot spells coincide with high

amplitude RRWPs (Fig. 3). Other regions over land where RRWPs are statistically associated with hot spell duration include

South America: southern Brazil, Bolivia, and parts of Argentina and Chile.

We have demonstrated the role of RRWPs in building persistent ridges during two cases of SEA heatwaves: the 2004 and

445   2009 heatwaves. Both heatwaves featured RRWPs comprised of transient Rossby waves, which were in phase regionally but

not hemisphere wide. Blocks were not directly observed over SEA, but the case studies suggest that blocks upstream and

downstream played an important role in initiating the Rossby wave packets and modulating their phase. We further

investigated the co-occurrence of RRWPs during the most persistent and extreme SEA heatwaves using the R-metric.

We find that days with R exceeding the 90th percentile, high R_{SEA} days, are associated with increased probabilities of being

450   part of a heatwave (0.19) compared to climatology. (0.13). These conditional probabilities have similar magnitudes as those

with remote drivers, e.g., Madden Julian oscillation (MJO), El ~~Nino~~Niño~~-~~Southern Oscillation (ENSO) (Parker et al.,

2014a). However, not all high R_{SEA} days are associated with heatwaves. Further investigations suggest that those high R_{SEA}

days, that are relevant for the SEA heatwaves, play a role in forming or sustaining the ridges over SEA. Such high R_{SEA} days

exhibit a circumglobal zonal ~~wavenumber~~wavenumbers 4 and 5 pattern in the PV composite and indicate a preferred phasing

455   of the waves. which is different from the DJF climatology. The high R_{SEA} days that do not coincide with SEA heatwave days

~~do not show preferred phasing (have~~ a ~~ridge or~~bimodal phase distribution in the WN4 component and result in a

~~trough)~~cyclonic PV anomaly over SEA. Therefore, R accompanied with information on the phasing of the wave packets

could be used as a diagnostic metric for SEA heatwaves. Upon filtering out days forming a cyclonic PV anomaly over SEA,

the conditional probability of SEA heatwave day given high R_{SEA} days increased to 0.34.

460   The following open questions remain: what is the role of blocks in initiating RRWPs and modulating their phase? The case

studies and the PV composites suggest that blocking might play an important role. What is the role of background flow in

setting up RRWPs and modulating their phase? The interaction of RRWPs with other well-known climate oscillation

patterns such as the ~~El Nino Southern Oscillation~~ENSO and the Southern Annular Mode also needs to be investigated

further. Better understanding of the interplay between these features might offer an opportunity to improve sub-seasonal

465 forecasts during RRWP events.

Appendix A: Comparison of _R_ anomalies for Southern Hemisphere and Northern Hemisphere

R anomalies are calculated for each day of year at each longitude from the mean of the day of the year mean. Therefore, the R anomalies at each longitude show variation with the mean of the day of year mean and have a seasonal pattern. The magnitude of the anomalies shows that there is larger variation in the values for the NH than the SH. Both the Southern and Northern Hemisphere _R_ fields show seasonality. Anomalies are highest for Northern Hemisphere boreal autumn and winter days. Interestingly, the Southern Hemisphere shows higher _R_ anomalies during austral summer days than winter days.
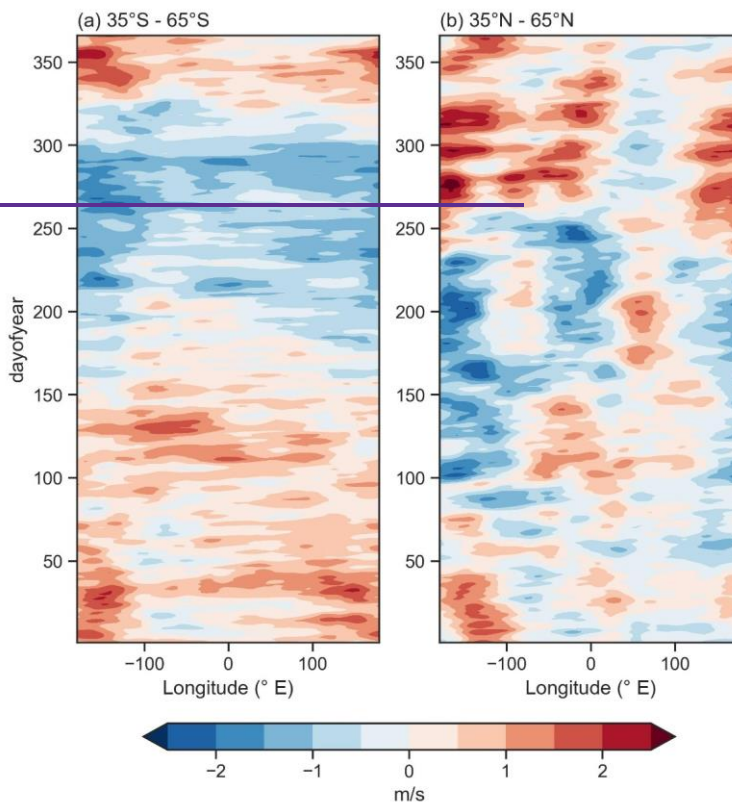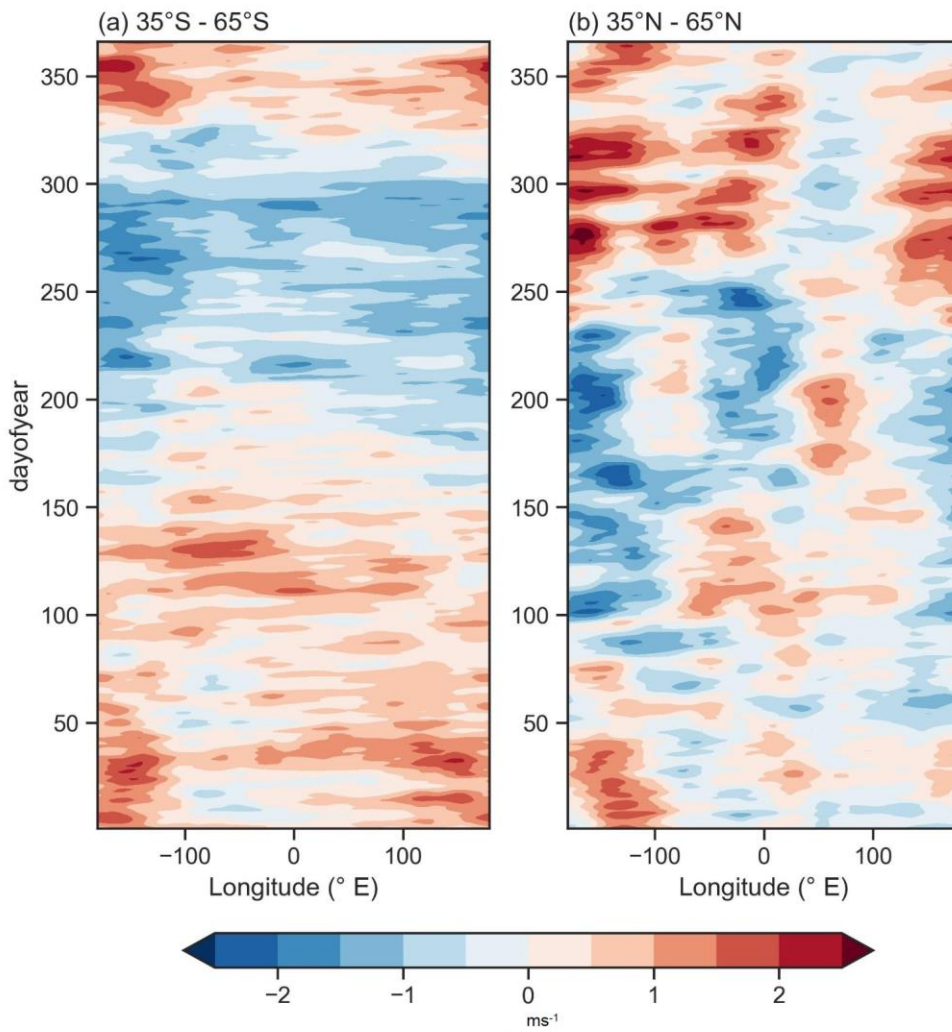
Figure A1: *R* anomalies for Southern and Northern hemispheres. Anomalies for day-of-year mean are calculated with respect to mean *R* fields.
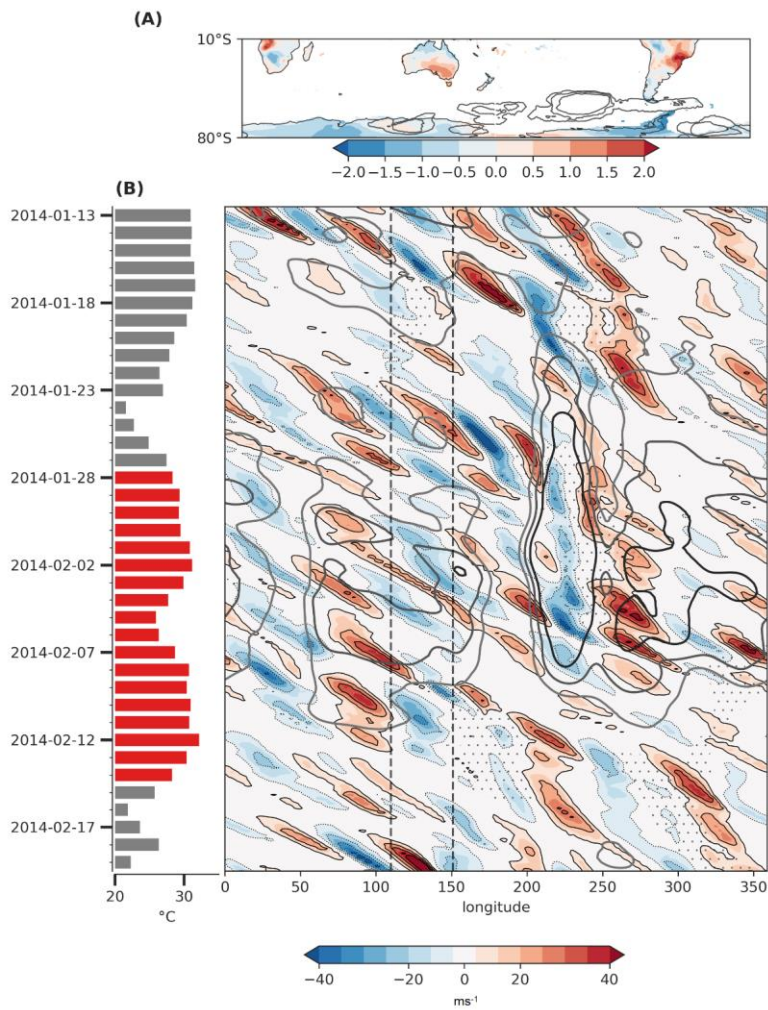
Figure B1: Same as in Fig. 4 but for January 2014 SEA heatwave.

480

Appendix C: Occurrence of High R_{SEA} on SEA heatwave days

	Days (DJF)	High R_{SEA} (days)	High R_{SEA} (ridges)
SEA heatwave days (SEA HD)	458457	67	57
SEA non-heatwave days	3062	285	107
Total	3520	352	164
Probability	$P_{heatwave}$ = 0.13	P (SEA HD | High R_{SEA}) = 0.19	P (SEA HD | High R_{SEA}) = 0.34

Inserted Cells

Table C1: Occurrence of High R_{SEA} on SEA heatwave days and the associated conditional probabilities of a heatwave given high R_{SEA}, where high R_{SEA} (ridges) in the last column is calculated from taking 90th percentile only from the days in DJF having an anticyclonic PV anomaly over SEA (30°S–45°S, 130°E–153°E).

Appendix D: PV composite for SEA heatwave days
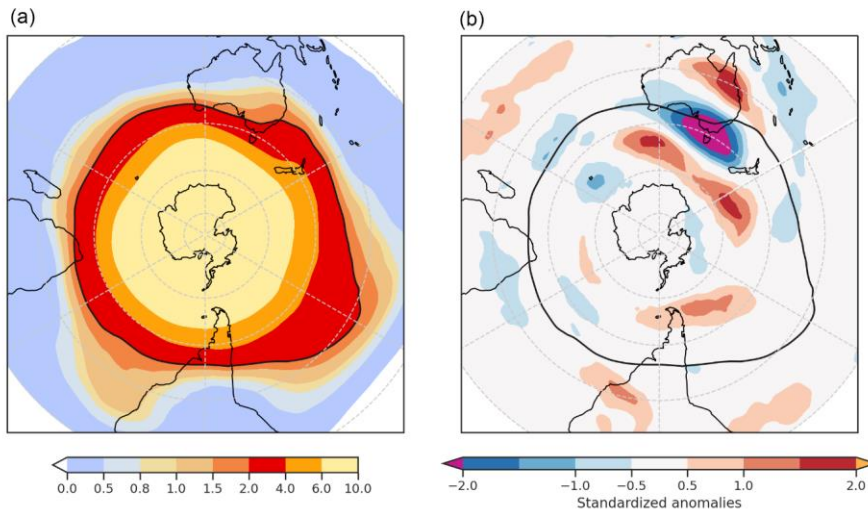
Figure D1: (a) PV composite mean at 350 K isentrope for SEA heatwave days, and (b) the respective anomalies with DJF mean climatology.

Figure D1 shows PV anomalies for all SEA heatwaves days identified in this study. The PV anomalies for SEA heatwaves feature anticyclonic PV anomalies over SEA with cyclonic PV anomalies to the north and south of it, that is similar to Fig. 2 in Parker et al. (2004) who show PV anomalies for Victorian heatwaves. However, the wavenumber pattern seen in Fig. 8a for SEA HD and high R_{SEA} is not clear for all SEA HD in Fig D1 (b).

Appendix E: **Relationship between blocks and RRWPs in the South Pacific and the Indian Ocean**

The figure shows four panels (a) N=617, (b) N=191, (c) N=592, (d) N=193 with Hovmöller composites.
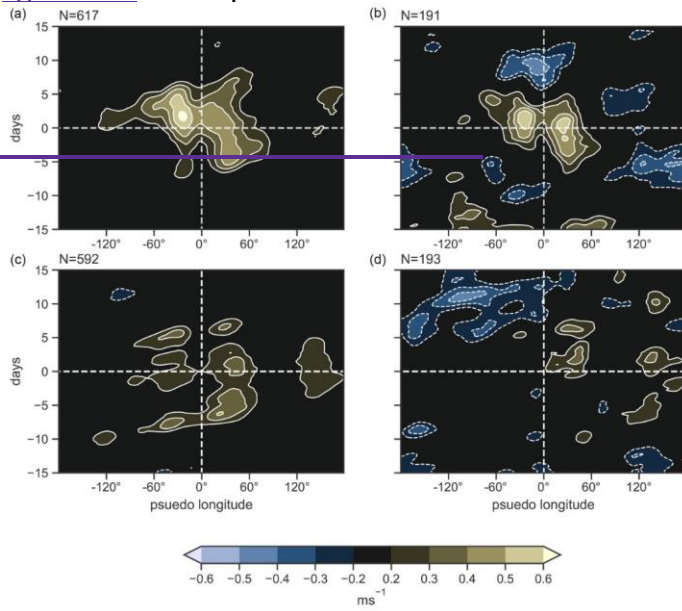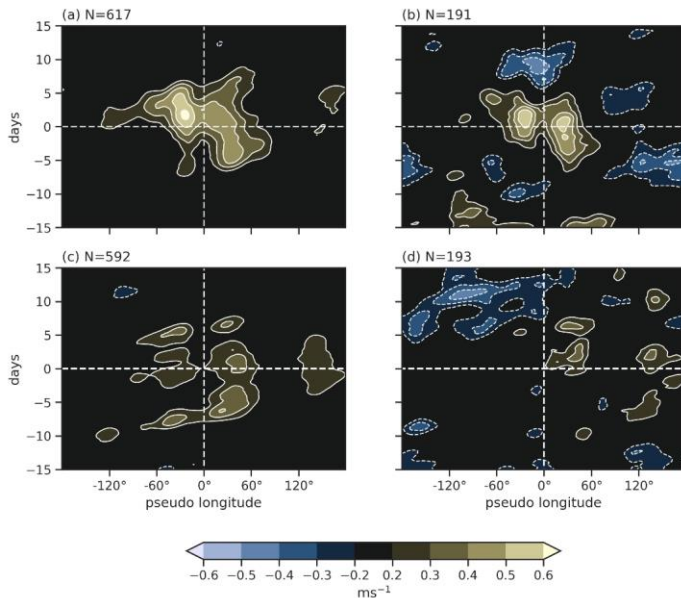
Figure ~~D1~~E1: **Time-lagged Hovmöller composites of *R* anomalies centred on the mean longitude and time of maximum amplitude of blocks located in Pacific Ocean (181–300° E, 30–80° S) in subplot (a) and (b), Indian Ocean (60–180° E, 30–80° S) in subplot (c) and (d). Left column includes blocks for all seasons and right shows for DJF. N denotes number of blocks for each category.**

500 To further analyse the spatial distribution of RRWPs relative to blocks in the SH, we focus on two longitudinal subdomains that show a high blocking frequency in the DJF climatological mean ~~(Fig. 11a):~~ the South Pacific Ocean (230 – 310 °E), and the Indian Ocean (0 –90 ° E). We use time-lagged composite *R* anomalies with respect to the centroid of the blocks at the time of the maximum blocking amplitude in the two domains similar to Röthlisberger et al. (2019; see Fig. 12 in their paper). Here, *R* anomalies are calculated with respect to the day-of-year climatology.

505 In the Pacific Ocean, blocks coincide with positive *R* anomalies in a longitudinal band from ~60° upstream to ~60° downstream of the blocks (Fig. ~~C1~~E1 a, b) from 5 to 8 days before the time of maximum blocking amplitude; this resembles a butterfly pattern, similar to blocks in the NH (Fig. 12, Röthlisberger et al., 2019). Similar to the NH, *R* anomalies in the Pacific Ocean are not high at the centroid of the block. This could be because the wavelength of the upper-level ridge

39

associated with the block may be too wide to be captured by the R metric because the R metric only has contributions from k

510 $=$ $=$4 and higher. R anomalies are consistent for DJF and blocks for all seasons in the Pacific. In contrast, in the Indian

Ocean, seasonal variation is seen in R anomalies (Fig. C1E1 c, d), where DJF blocks located in DJF show R anomalies

downstream of the centroid of the block only and possibly show weak association with RRWPs.

Code and data availability

Code for calculating R metric is available on GitHub (Ali and Röthlisberger, 2021). The code for blocking dataset can be

515 downloaded from https://github.com/marco-rohrer/TM2D. ACORN-SAT data is available at

http://www.bom.gov.au/climate/data/acorn-sat/#tabs=ACORN%E2%80%90SAT. The ERA-I reanalysis dataset used can be

downloaded from https://apps.ecmwf.int/datasets/data/interim-full-daily/levtype=pl/.

Author Contributions

SMA performed the formal analysis and wrote the first draft. All the authors contributed to the interpretation and discussion

520 of the results and in review of the draft.

Competing Interests

The authors declare that they have no conflict of interest.

41

References

Ali, M. and Röthlisberger, M.: avatar101/R-metric: (Version v1.1), Zenodo, https://doi.org/10.5281/zenodo.5742810, 2021.

535   Ali, S. M., Martius, O., and Röthlisberger, M.: Recurrent Rossby Wave Packets Modulate the Persistence of Dry and Wet Spells Across the Globe, Geophys. Res. Lett., 48, e2020GL091452, https://doi.org/https://doi.org/10.1029/2020GL091452, 2021.

Barriopedro, D., Fischer, E. M., Luterbacher, J., Trigo, R. M., and ~~Garc\'\ia~~Garcia-Herrera, R.: The Hot Summer of 2010: Redrawing the Temperature Record Map of Europe, Science (80-.)., 332, 220–224, https://doi.org/10.1126/science.1201224, 2011.

Barton, Y., Giannakaki, P., Von Waldow, H., Chevalier, C., Pfahl, S., & Martius, O: Clustering of regional-scale extreme precipitation

540   events in southern Switzerland. Monthly Weather Review, 144(1), 347–369., 2016.

Benjamini, Y. and Hochberg, Y.: Controlling the False Discovery Rate: A Practical and Powerful Approach to Multiple Testing, Source: Journal of the Royal Statistical Society. Series B (Methodological), 289–300 pp., 1995.

Black, E., Blackburn, M., Harrison, G., Hoskins, B., and Methven, J.: Factors contributing to the summer 2003 European heatwave, 59, 217–223, https://doi.org/10.1256/wea.74.04, 2004.

545   Coumou, D., Robinson, A., and Rahmstorf, S.: Global increase in record-breaking monthly-mean temperatures, Clim. Change, 118, 771–782, https://doi.org/10.1007/s10584-012-0668-1, 2013.

Davies, H. C.: Weather chains during the 2013/2014 winter and their significance for seasonal prediction, Nat. Geosci., https://doi.org/10.1038/ngeo2561, 2015.

Dee, D. P., Uppala, S. M., Simmons, A. J., Berrisford, P., Poli, P., Kobayashi, S., Andrae, U., Balmaseda, M. A., Balsamo, G., Bauer, P.,

550   Bechtold, P., Beljaars, A. C. M., van de Berg, L., Bidlot, J., Bormann, N., Delsol, C., Dragani, R., Fuentes, M., Geer, A. J., Haimberger, L., Healy, S. B., Hersbach, H., Hólm, E. V., Isaksen, L., Kållberg, P., Köhler, M., Matricardi, M., Mcnally, A. P., Monge-Sanz, B. M., Morcrette, J. J., Park, B. K., Peubey, C., de Rosnay, P., Tavolato, C., Thépaut, J. N., and Vitart, F.: The ERA-Interim reanalysis: Configuration and performance of the data assimilation system, Q. J. R. Meteorol. Soc., 137, 553–597, https://doi.org/10.1002/qj.828, 2011.

555   Drouard, M. and Woollings, T.: Contrasting Mechanisms of Summer Blocking Over Western Eurasia, Geophys. Res. Lett., 45, 12,040-12,048, https://doi.org/10.1029/2018GL079894, 2018.

Engel CB, Lane TP, Reeder MJ, Rezny M.: The meteorology of Black Saturday, Q. J. R.Meteorol. Soc. 139: 585–599, https://doi.org/10.1002/qj.1986, 2013.

Fragkoulidis, G., Wirth, V., Bossmann, P., and Fink, A. H.: Linking Northern Hemisphere temperature extremes to Rossby wave packets,

560   Q. J. R. Meteorol. Soc., 144, 553–566, https://doi.org/10.1002/qj.3228, 2018.

42

Green, J. S. A.: The weather during July 1976: Some dynamical considerations of the drought. Weather, 32, 120-126, 1977.

Hoskins, B.J., McIntyre, M.E., and Robertson, A.W.: On the use and significance of isentropic potential vorticity maps. Q.J.R. Meteorol. Soc., 111: 877-946. https://doi.org/10.1002/qj.49711147002, 1985.

Hoskins, B. J. and Sardeshmukh, P. D.: A Diagnostic Study of the Dynamics of the Northern Hemisphere Winter of 1985-86, Q. J. R. Meteorol. Soc., 113, 759–778, https://doi.org/10.1002/qj.49711347705, 1987.

Hughes, L., Steffen, W., Mullins, G., Dean, A., Weisbrot, E., and Rice, M.: Summer of crisis, 2020. Insurance Council Of Australia, 2020. Insurance Council Of Australia: INSURANCE COUNCIL OF AUSTRALIA, 2020.

Karoly D. J.: The recent bushfires and extreme heat wave in southeast Australia. Bull. Aust. Meteorol. Oceanogr. Soc., 22(1):10-3, 2009.

King, M.J., and Reeder, M.J.: Extreme heat events from an object viewpoint with application to south-east Australia. Int J Climatol.; 41: 2693– 2709, https://doi.org/10.1002/joc.6984, 2021.

Kautz, L.-A., Martius, O., Pfahl, S., Pinto, J. G., Ramos, A. M., Sousa, P. M., and Woollings, T.: Atmospheric blocking and weather extremes over the Euro-Atlantic sector – a review, Weather Clim. Dynam., 3, 305–336, https://doi.org/10.5194/wcd-3-305-2022, 2022.

Kornhuber, K., Petoukhov, V., Petri, S., Rahmstorf, S., and Coumou, D.: Evidence for wave resonance as a key mechanism for generating high-amplitude quasi-stationary waves in boreal summer, Clim. Dyn., 49, 1961–1979, https://doi.org/10.1007/s00382-016-3399-6, 2017.

Kornhuber, K., Coumou, D., Vogel, E., Lesk, C., Donges, J. F., Lehmann, J., and Horton, R. M.: Amplified Rossby waves enhance risk of concurrent heatwaves in major breadbasket regions, Nat. Clim. Chang., 10, 48–53, https://doi.org/10.1038/s41558-019-0637-z, 2020.

Lenggenhager, S., Martius, O. Atmospheric blocks modulate the odds of heavy precipitation events in Europe. Clim Dyn 53, 4155–4171, https://doi.org/10.1007/s00382-019-04779-0, 2019.

Marshall, A. G., Debra Hudson, M. C. Wheeler, O. Alves, H. H. Hendon, M. J. Pook, and J. S. Risbey. "Intra-seasonal drivers of extreme heat over Australia in observations and POAMA-2." Climate dynamics 43, no. 7: 1915-1937, 2014.

Martius, O., C. Schwierz, and H. C. Davies.: Tropopause-level waveguides, J. Atmos.Sci., 67, 866–879, https://doi.org/10.1175/2009JAS2995.1, 2010.

Martius, O., Wehrli, K., & Rohrer, M.: Local and Remote Atmospheric Responses to Soil Moisture Anomalies in Australia, Journal of Climate, 34(22), 9115-9131, https://doi.org/10.1175/JCLI-D-21-0130.1, 2021.

Masson-Delmotte, V., P. Zhai, A. Pirani, S. L. Connors, C. Péan, S. Berger, N. Caud, Y. Chen, L. Goldfarb, M.I. Gomis, M. Huang, K. Leitzell, E. Lonnoy, J. B. R., and Matthews, T.K. Maycock, T. Waterfield, O. Yelekçi, R. Yu, and B. Z. (eds. .: IPCC, 2021: Climate Change 2021: The Physical Science Basis. Contribution of Working Group I to the Sixth Assessment Report of the Intergovernmental Panel on Climate Change, https://www.ipcc.ch/report/ar6/wg1/#FullReport, 2021.

National Climate Centre (2004) Eastern Australia experiences record February heatwave. Bull. Aust. Meteorol. Oceanogr Soc. 17:27–29

590   O'Brien, L. and Reeder, M. J.: Southern Hemisphere summertime Rossby waves and weather in the Australian region, Q. J. R. Meteorol. Soc., 143, 2374–2388, https://doi.org/10.1002/qj.3090, 2017.

Parker, T., Berry, G. J., Reeder, M. J., and Nicholls, N.: Modes of climate variability and heat waves in Victoria, southeastern Australia, Geophys. Res. Lett., 41, 6926–6934, https://doi.org/10.1002/2014GL061736, 2014a.

Parker, T., Berry, G. J., and Reeder, M. J.: The Structure and Evolution of Heat Waves in Southeastern Australia, J. Clim., 27, 5768–5785,

595   https://doi.org/10.1175/JCLI-D-13-00740.1, 2014b.

Parker, T., Quinting, J., and Reeder, M.: The synoptic-dynamics of summertime heatwaves in the Sydney area (Australia), J. South. Hemisph. Earth Syst. Sci., 69, 116, https://doi.org/10.1071/es19004, ~~2019~~2020.

Pelly, J. L., & Hoskins, B. J.: A New Perspective on Blocking, Journal of the Atmospheric Sciences, 60(5), 743-755, https://doi.org/10.1175/1520-0469(2003)060<0743:ANPOB>2.0.CO;2 , 2003.

600   Perkins-Kirkpatrick, S. E. and Lewis, S. C.: Increasing trends in regional heatwaves, Nat. Commun., 11, 1–8, 2020.

Petoukhov, V., Rahmstorf, S., Petri, S., and Schellnhuber, H. J.: Quasiresonant amplification of planetary waves and recent Northern Hemisphere weather extremes, Proc. Natl. Acad. Sci. U. S. A., 110, 5336–5341, https://doi.org/10.1073/pnas.1222000110, 2013.

Pfahl, S. and Wernli, H.: Quantifying the relevance of atmospheric blocking for co-located temperature extremes in the Northern Hemisphere on (sub-)daily time scales, Geophys. Res. Lett., 39, 1–6, https://doi.org/10.1029/2012GL052261, 2012.

605   Quandt, L.-A., Keller, J. H., Martius, O., and Jones, S. C.: Forecast variability of the blocking system over Russia in summer 2010 and its impact on surface conditions, Weather Forecast., 32, 61–82, 2017.

Quinting, J. F., and Reeder, M. J,: Southeastern Australian Heat Waves from a Trajectory Viewpoint, Mon. Weather Rev., 145, 4109–4125, https://doi.org/10.1175/MWR-D-17-0165.1, 2017.

Risbey, J. S., O'Kane, T. J., Monselesan, D. P., Franzke, C. L. E., and Horenko, I~~.~~.: On the dynamics of Austral heat waves. *Journ. of*

610   *Geophys. Res.: Atmos.*, 123, 38– 57. https://doi.org/10.1002/2017JD027222, 2018.

Rohrer, M., ~~Brönnimann, S.,~~ Martius, O., Raible, C. C., ~~Wild, M.,~~ and ~~Compo, G. P.: Representation~~Brönnimann, S.: Sensitivity of ~~extratropical cyclones, blocking anticyclones,~~Blocks and ~~alpine circulation types~~Cyclones in ~~multiple reanalyses~~ERA5 to Spatial Resolution and ~~model simulations, J. Clim., 31, 3009–3031,~~Definition. Geophysical Research Letters, 47, e2019GL085582. https://doi.org/10.~~1175/JCLI-D-17-0350.1, 2018~~1029/2019GL085582, 2020.

615   Röthlisberger, M., Martius, O., & Wernli, H.: Northern Hemisphere Rossby Wave Initiation Events on the Extratropical Jet—A Climatological Analysis, Journal of Climate, 31(2), 743–760, https://journals.ametsoc.org/view/journals/clim/31/2/jcli-d-17-0346.1.xml,

44

2018.

Röthlisberger, M., Frossard, L., Bosart, L. F., Keyser, D., and Martius, O.: Recurrent synoptic-scale Rossby wave patterns and their effect on the persistence of cold and hot spells, J. Clim., 32, 3207–3226, https://doi.org/10.1175/JCLI-D-18-0664.1, 2019.

620 Schneidereit, A., Schubert, S., Vargin, P., Lunkeit, F., Zhu, X., Peters, D. H. W., and Fraedrich, K.: Large-Scale Flow and the Long-Lasting Blocking High over Russia: Summer 2010, Mon. Weather Rev., 140, 2967–2981, https://doi.org/10.1175/MWR-D-11-00249.1, 2012.

Schwierz, C., Croci-Maspoli, M., and Davies, H. C.: Perspicacious indicators of atmospheric blocking, Geophys. Res. Lett., 31, 6, https://doi.org/10.1029/2003gl019341, 2004.

625 Seneviratne, S.I., Corti, T., Davin, E.L., Hirschi, M., Jaeger, E.B., Lehner, I., Orlowsky, B. and Teuling, A.J.: Investigating soil moisture–climate interactions in a changing climate: A review. Earth-Science Reviews, 99(3-4), pp.125-161., 2010.

Shepherd, T. G.: Atmospheric circulation as a source of uncertainty in climate change projections, Nat. Geosci., 7, 703–708, https://doi.org/10.1038/NGEO2253, 2014.

Shutts, G. J.: The propagation of eddies in diffluent jetstreams: Eddy vorticity forcing of 'blocking' flow fields, Q. J. R. Meteorol. Soc.,
630 https://doi.org/10.1002/qj.49710946204, 1983.

Sousa, P. M., D. Barriopedro, R. García-Herrera, T. Woollings, and R. M. Trigo: A new combined detection algorithm for blocking and subtropical ridges. J. Clim, 34, 18, 7735-7758, https://doi.org/10.1175/JCLI-D-20-0658.1, 2021.

Teng, H., Branstator, G., Meehl, G. A., and Washington, W. M.: Projected intensification of subseasonal temperature variability and heat waves in the Great Plains, Geophys. Res. Lett., 43, 2165–2173, https://doi.org/https://doi.org/10.1002/2015GL067574, 2016.

635 Trigo, R. M., Trigo, I. F., DaCamara, C. C., and Osborn, T. J.: Climate impact of the European winter blocking episodes from the NCEP/NCAR Reanalyses, Clim. Dyn., 23, 17–28, https://doi.org/10.1007/s00382-004-0410-4, 2004.

VBRC: Final   report   of   the   Victorian   Bushfires   Royal   Commission.   [Available   online   at http://www.royalcommission.vic.gov.au/Commission-Reports.], 2010.

Wehrli, K., Guillod, B. P., Hauser, M., Leclair, M., and Seneviratne, S. I.: Identifying Key Driving Processes of Major Recent Heat
640 Waves, J. Geophys. Res. Atmos., 124, 11746–11765, https://doi.org/https://doi.org/10.1029/2019JD030635, 2019.

Wernli, H. and Schwierz, C.: Surface cyclones in the ERA-40 dataset (1958-2001). Part I: Novel identification method and global climatology, J. Atmos. Sci., 63, 2486–2507, https://doi.org/10.1175/JAS3766.1, 2006.

White, R. H., Kornhuber, K., Martius, O., and Wirth, V.: From Atmospheric Waves to Heatwaves: A Waveguide Perspective for Understanding and Predicting Concurrent, Persistent and Extreme Extratropical Weather, Bull. Am. Meteorol. Soc., 1–35,

645 https://doi.org/10.1175/BAMS-D-21-0170.1, 2021.

Wilks, D. S.: "The stippling shows statistically significant grid points": How research results are routinely overstated and overinterpreted, and what to do about it, https://doi.org/10.1175/BAMS-D-15-00267.1, 2016.

Wirth, V., Riemer, M., Chang, E. K. M., and Martius, O.: Rossby Wave Packets on the Midlatitude Waveguide — A Review, Mon. Weather Rev., MWR-D-16-0483.1, https://doi.org/10.1175/MWR-D-16-0483.1, 2018.

650 Zimin, A. V., Szunyogh, I., Patil, D. J., Hunt, B. R., and Ott, E.: Extracting Envelopes of Rossby Wave Packets, Mon. Weather Rev., https://doi.org/10.1175/1520-0493(2003)131<1011:EEORWP>2.0.CO;2, 2003.

Wolf, G., Brayshaw, D.J., Klingaman, N.P. and Czaja, A.: Quasi-stationary waves and their impact on European weather and extreme events. Quarterly Journal of the Royal Meteorological Society, 144(717), pp.2431-2448, 2018.